Single-shot grating-based x-ray differential phase contrast imaging with a modified analyzer grating*

Chen-Xi Wei(卫晨希)[1], Zhao Wu(吴朝)[1,†], Faiz Wali[1], Wen-Bin Wei(魏文彬)[1], Yuan Bao(鲍园)[2], Rong-Hui Luo(骆荣辉)[1], Lei Wang(王磊)[1], Gang Liu(刘刚)[1], and Yang-Chao Tian(田扬超)[1,‡]

[1] *National Synchrotron Radiation Laboratory, University of Science and Technology of China, Hefei* 230029, *China*
[2] *Shanghai United Imaging Healthcare Co. Ltd., Shanghai* 201807, *China*

(Received 25 April 2017; revised manuscript received 6 June 2017; published online 10 September 2017)

X-ray grating interferometer has attracted widely attention in the past years due to its capability in achieving x-ray phase contrast imaging with low brilliance source. However, the widely used phase stepping information extraction method reduces system stability and prolongs data acquisition time by several times compared with conventional x-ray absorption-based imaging. The mechanical stepping can be avoided by using a staggered grating, but at the cost of low vertical spatial resolution. In this paper, employing a modified staggered grating and the angular signal radiography, we proposed a single-shot grating-based x-ray differential phase contrast imaging with decent vertical spatial resolution. The theoretical framework was deduced and proved by numerical experiments. Absorption, phase, and scattering computed tomography can be performed without phase stepping. Therefore, we believe this fast and highly stable imaging method with decent resolution would be widely applied in x-ray grating-based phase contrast imaging.

Keywords: x-ray phase contrast imaging, single-shot, decent resolution, staggered grating, computed tomography

PACS: 87.59.–e, 42.30.Rx, 87.57.Q–, 41.50.+h **DOI:** 10.1088/1674-1056/26/10/108701

1. Introduction

Grating-based x-ray differential phase contrast imaging has been widely researched over the past decades and has shown many advantages, especially high sensitivity, in soft tissue imaging,[1–7] complementing conventional absorption-based imaging. It provides a promising method in clinical diagnosis, biological researches and industrial nondestructive testing. Because the detected projection images are the mixture of absorption, refraction and scattering, information extraction method is a critical step in signal processing. Various methods have been developed,[8–12] among of which phase stepping procedure is widely used.[13,14] When one of the gratings shifts laterally, the x-ray intensities recorded in each pixel oscillate as a function of the relative grating position, known as the Shifting Curve (SC), which can be approximated as a cosine curve. The phase stepping procedure needs to move one of the gratings twice or more in order to retrieve three signals. Thus long exposure time and mechanical instability prevent its wide applications.

In order to reduce the data acquisition time of phase contrast imaging, many efforts have been made.[8–10,15–19] Ge *et al.*[18] designed and introduced a staggered analyzer grating in 2014, which was divided into many rows and the height of each row was the same as detector pixel. In this method, x-ray intensities recorded from several neighboring detector rows were used to extract information, and the number of rows could be defined as an extraction unit. Meanwhile, any two adjacent grating rows in one extraction unit had a fixed displacement. Using this staggered structure, a single-shot projection image can be used to retrieve absorption, refraction and scattering signals simultaneously. An extraction unit of the staggered analyzer grating should contain three rows at least to meet the extraction requirement. However, the increasing rows in one extraction unit has a negative influence on the vertical spatial resolution. Li *et al.*[20] introduced an alternative approach, termed angular signal radiography (ASR), to describe the imaging process of x-ray grating imaging (XGI) system in 2016, angular signal response function (ASRF) was used to describe the imaging system. In that paper, four specified positions, named valley-SC, upslope-SC, peak-SC, and downslope-SC respectively, of the SC were chosen to extract the absorption, refraction and scattering information. Because of the characteristics of these positions, three of them are enough to extract signals. However, the analyzer grating still needs to be moved twice, which reduces the image quality due to mechanical errors and increases exposure time compared with conventional absorption-based imaging modality. There-

*Project supported by the National Natural Science Foundation of China (Grant Nos. 11275204, 11475175, and 11405175), the China Postdoctoral Science Foundation (Grant No. 2017M612097), and the Fundamental Research Funds for the Central Universities (Grant No. WK2310000065).

†Corresponding author. E-mail: wuzhao@ustc.edu.cn
‡Corresponding author. E-mail: ychtian@ustc.edu.cn

© 2017 Chinese Physical Society and IOP Publishing Ltd

fore, developing practical phase contrast imaging methods free of mechanical stepping and with decent spatial resolution becomes very important and meaningful.

In this manuscript, we introduce a single-shot grating-based x-ray differential phase contrast imaging with better vertical spatial resolution compared with the reported results.[18] Meanwhile, this single-shot imaging system reduces mechanical errors compared with those employing the traditional phase stepping method.

2. Theoretical framework of the novel imaging system

Firstly, we introduce a modified staggered analyzer grating, then the principle and theoretical framework of the novel imaging system using this new staggered grating are presented.

2.1. Introduction of the staggered gratings

To minimize the errors caused by mechanical stepping and the spatial resolution decrease in the vertical direction, a modified staggered analyzer grating is designed shown in Fig. 1(a), accompanying with the original staggered analyzer grating in Fig. 1(b). Compared with the original one, the displacement of adjacent rows maintains a quarter of its period, while two but not four rows are defined as one extraction unit. The height d of the rows equals to 50 μm, which is the same as the size of the detector pixel.

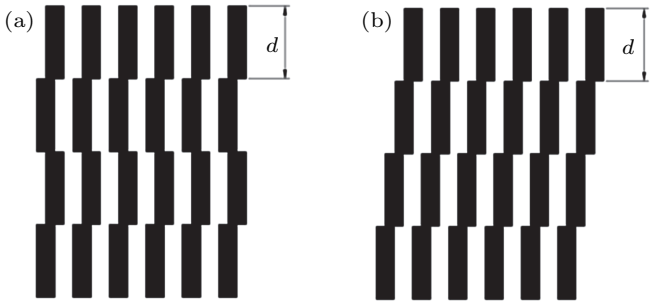


Fig. 1. (a) Structures of the proposed staggered grating with two rows in one extraction unit and (b) the original staggered grating with four rows in one extraction unit.

2.2. Principle and theoretical framework of the imaging system

Figure 2(a) illustrates the schematic diagram of single-shot phase contrast imaging system using the modified staggered analyzer grating, which replaces the original staggered analyzer grating in Ref. [18]. The imaging system consists of an x-ray source, a $\pi/2$ phase grating G1, an absorption staggered analyzer grating G2 and an image detector. G2 is positioned at the first fraction Talbot distance of G1. The normalized shifting curve as a function of the relative position between G1 and G2 is shown in Fig. 2(b).

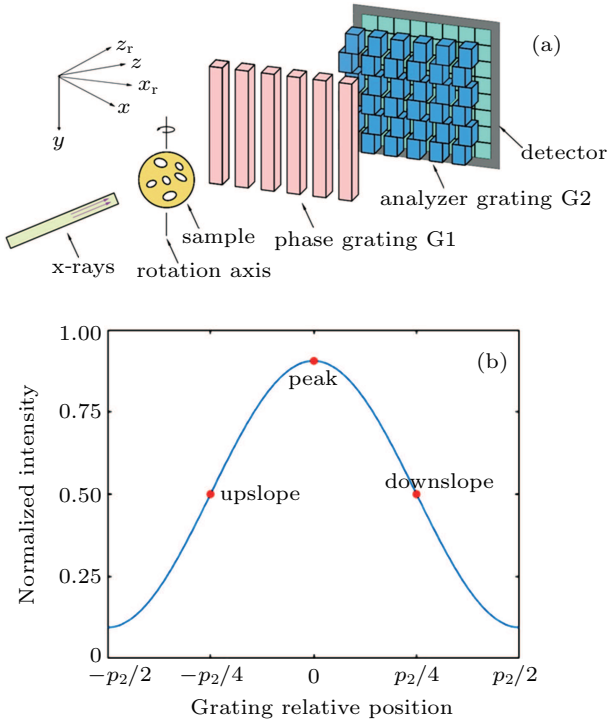


Fig. 2. (color online) (a) Illustration of single-shot x-ray grating interferometer. (b) Normalized shifting curve as a function of the relative position of the phase grating and the analyzer grating.

According to the Beer–Lambert law, the attenuation of the sample is the integral of absorption coefficients along x-ray path

$$M(x_r, y) = \int \mu(x, y, z)\, \mathrm{d}z_r. \tag{1}$$

According to the relationship between the refraction angle (θ) induced by the sample and the phase shift $\Phi(x_r, y)$ of the sample, the refraction angle can be expressed as

$$\theta(x_r, y) = \frac{\lambda}{2\pi}\frac{\partial \Phi(x_r, y)}{\partial x_r} = -\int \frac{\partial \delta(x, y, z)}{\partial x_r}\mathrm{d}z_r. \tag{2}$$

For the ultra-small angle scattering, it has been claimed that the second moment of scattering angle distribution describing the broadening of the x-ray was actually the scattering information.[21–23]

$$\begin{aligned}\sigma^2(x_r, y) &= \int S(x, y, z)\, \mathrm{d}z_r \\ &= \int \left[\frac{\rho_n(x, y, z)\, \sigma_s(x, y, z)}{2\alpha_p}\right] \mathrm{d}z_r,\end{aligned} \tag{3}$$

where S represents the scattering coefficient, ρ_n is the density of the sample, σ_s is the scattering cross section and α_p means angular beam broadening due to a single scatterer.

Using the staggered grating shown in Fig. 1(a), when one row (the odd row is considered in this paper) is positioned at the downslope of the shifting curve, its adjacent row should be at the peak or valley of the shifting curve. With the sample or imaging system rotated 180°, the upslope image and peak or valley image are acquired. Thus absorption, differential phase and scattering signals at rotation angle of φ can

be extracted by Eqs. (4)–(6) according to the angular signal radiography.[20] The derivation of the equations has been presented in Appendix A. It should be mentioned that when using the proposed staggered grating displayed in Fig. 1(a), two adjacent rows in the vertical direction have been used as an extraction unit, while using the previous staggered grating displayed in Fig. 1(b), an extraction unit are four adjacent rows. In parallel beam geometry, the vertical spatial resolution in the proposed imaging system is improved twice compared with that in the previous imaging system. Then, a fast and simple x-ray phase tomography with decent vertical resolution can be performed.

$$M_\varphi(x_r,2y-1) = M_\varphi(x_r,2y) = \ln\left[\frac{I^{\rm b}_\varphi(x_r,2y-1)+I^{\rm b}_{\varphi+\pi}(-x_r,2y-1)}{I^{\rm s}_\varphi(x_r,2y-1)+I^{\rm s}_{\varphi+\pi}(-x_r,2y-1)}\right], \tag{4}$$

$$\begin{aligned}\theta_\varphi(x_r,2y-1) &= \theta_\varphi(x_r,2y) = -\frac{p}{2\pi D}\left[\arctan\frac{I^{\rm s}_{\varphi+\pi}(-x_r,2y-1)-I^{\rm s}_\varphi(x_r,2y-1)}{I^{\rm s}_\varphi(x_r,2y-1)+I^{\rm s}_{\varphi+\pi}(-x_r,2y-1)-2I^{\rm s}_\varphi(x_r,2y)}\right]\\ &\quad+\frac{p}{2\pi D}\left[\arctan\frac{I^{\rm b}_{\varphi+\pi}(-x_r,2y-1)-I^{\rm b}_\varphi(x_r,2y-1)}{I^{\rm b}_\varphi(x_r,2y-1)+I^{\rm b}_{\varphi+\pi}(-x_r,2y-1)-2I^{\rm b}_\varphi(x_r,2y)}\right],\end{aligned} \tag{5}$$

$$\begin{aligned}\sigma^2_\varphi(x_r,2y-1) &= \sigma^2_\varphi(x_r,2y)\\ &= -\frac{p^2}{2\pi^2D^2}\ln\left[\frac{\sqrt{(I^{\rm s}_{\varphi+\pi}(-x_r,2y-1)-I^{\rm s}_\varphi(x_r,2y-1))^2+(I^{\rm s}_\varphi(x_r,2y-1)+I^{\rm s}_{\varphi+\pi}(-x_r,2y-1)-2I^{\rm s}_\varphi(x_r,2y))^2}}{V_0(I^{\rm s}_\varphi(x_r,2y-1)+I^{\rm s}_{\varphi+\pi}(-x_r,2y-1))}\right]\\ &\quad+\frac{p^2}{2\pi^2D^2}\ln\left[\frac{\sqrt{(I^{\rm b}_{\varphi+\pi}(-x_r,2y-1)-I^{\rm b}_\varphi(x_r,2y-1))^2+(I^{\rm b}_\varphi(x_r,2y-1)+I^{\rm b}_{\varphi+\pi}(-x_r,2y-1)-2I^{\rm b}_\varphi(x_r,2y))^2}}{V_0(I^{\rm b}_\varphi(x_r,2y-1)+I^{\rm b}_{\varphi+\pi}(-x_r,2y-1))}\right],\end{aligned} \tag{6}$$

where $I^{\rm b}$ and $I^{\rm s}$ are recorded x-ray intensities without and with the sample in the imaging system respectively. p is the period of the analyzer grating, and D is the first fraction Talbot distance, equals to $p^2/2\lambda$, with λ the wavelength of the incoming x ray. V_0 is the visibility of the shifting curve.

3. Simulations

To show the advantage of the proposed imaging system, the phantom used here is the well-known three dimensional Shepp–Logan phantom filled with four different materials. In this part, we introduce the parameters of the system and the sample first, then the quantitative comparisons of the extracted information and the three-dimensional (3D) reconstruction have also been performed.

3.1. The system parameters and the sample

The simulations using the MATLAB software were performed, x-ray energy of 20 keV was designed, which can be acquired from the synchrotron radiation light source. The pixel of the detector was 50 μm×50 μm, and the periods of phase grating (G1) and analyzer grating (G2) equaled to 4 μm. The phantom shown in Fig. 3(a) consisted of four different materials and its volume was 12.8 mm×12.8 mm×12.8mm. Figure 3(b) exhibits its middle coronal slice, which will be compared with its reconstructed image in Subsection 4.2. Names and parameters of the four materials are listed in Table 1. They were rendered by green (parylene-N), red (polycarbonate), dark blue (PMMA-formvar), and sky blue (water) respectively in Fig. 3.

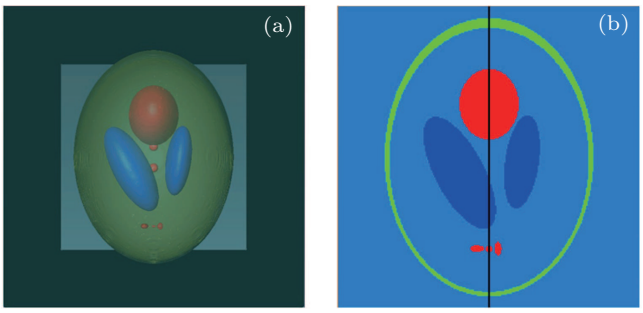


Fig. 3. (color online) (a) The 3D rendering of the phantom used in the simulation, and (b) its middle coronal slice. The four materials are parylene-N (green), polycarbonate (red), PMMA-formvar (dark blue), and water (sky blue) respectively.

Table 1. The composition of the sample and their complex refraction indexes at 20 keV.

Materials	Chemical formulae	$\delta/10^{-7}$	$\beta/10^{-10}$
Parylene-N	C_8H_8	6.19682055	1.99766786
Polycarbonate	$C_{16}H_{14}O_3$	6.56665406	2.58399607
PMMA-formvar	$C_5H_8O_2$	6.66553376	2.85367757
Water	H_2O	5.76620721	3.46201373

3.2. Data acquisition and 3D reconstruction

During the imaging process, the detector recorded the x-ray intensities without the sample in the imaging system (I^{b}) first, then recorded the x-ray intensities (I^{s}) with the sample in the system. Finally, equations (4)–(6) were used to extract absorption, refraction and scattering information.

The sample mentioned above in Fig. 3(a) were used to simulate the imaging process with the proposed imaging system and that with the previous imaging system. In phase tomography, the sample was scanned with 1° increment within 360°, and the imaging process was implemented to acquire two sets of images with and without the sample. First, we implemented the intuitionistic and quantitative comparisons of the extracted information between the two imaging systems employing the analyzer gratings respectively shown in Figs. 1(a) and 1(b), then the 3D reconstruction were performed using conventional back-projection algorithm with Ram-Lak and Hilbert filters.

4. Results and discussion

4.1. Decent vertical spatial resolution

Figure 4 shows the information of the sample at the rotation angle of 0° and figure 5 displays the quantitative comparisons of the theoretical values and the extracted information in the vertical spatial direction, which have been marked white in Figs. 4(a)–4(c), using the proposed imaging system employing the modified staggered analyzer grating shown in Fig. 1(a) and the previous imaging system using the original staggered analyzer grating displayed in Fig. 1(b).

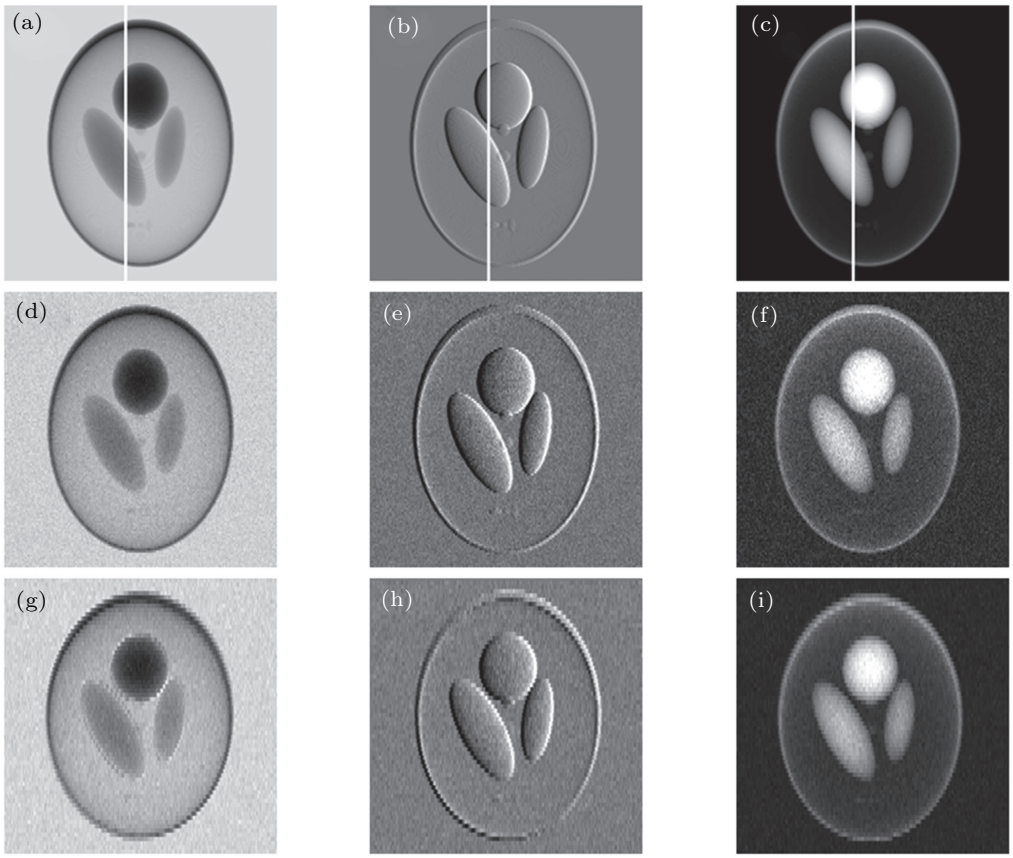


Fig. 4. The information of the sample at the rotation angle of 0°. Panels (a)–(c) are the original information, panels (d)–(f) are the information extracted using the modified staggered analyzer grating, and panels (g)–(i) are the information extracted using the original staggered analyzer grating.

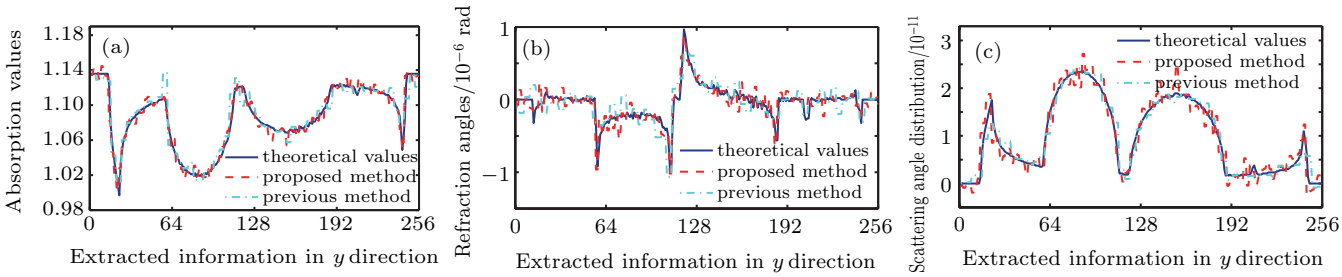


Fig. 5. (color online) Quantitative comparisons of the theoretical values and the extracted information respectively using the modified staggered analyzer grating and the original staggered analyzer grating: the absorption values (a), refraction angles (b), and scattering angle distribution (c).

From the extracted information shown in Fig. 4, it can be intuitively seen that the imaging system using the modified staggered analyzer grating has better vertical spatial resolution compared with that using the original staggered analyzer grating. From the quantitative comparisons displayed in Fig. 5, the extracted information using the proposed imaging system fits the theoretical values much better than that using the previous imaging system, which also quantitatively shows the proposed imaging system can improve the vertical spatial resolution compared with the previous one. It can be concluded that the spatial resolution is improved twice in parallel beam geometry, because the extraction unit of the proposed method is half of that of the previous method.

According to the comparisons shown above, we can find the proposed imaging system is more effective and can improve the vertical spatial resolution compared with the previous imaging system.

4.2. Fast and simple computed tomography

Figures 6(a)–6(c) display the reconstructed images of the middle coronal slice of the simulated phantom shown in Fig. 3(b) using the proposed imaging system, and figures 6(d)–6(f) show the counterparts using the previous imaging system. Profile comparisons of the line shown in Fig. 3(b) are achieved in Fig. 7. From the reconstruction results of the proposed phase contrast imaging, the good agreement between the reconstructed values and the theoretical values confirms the validity of the proposed method. While serious artifacts appear in those of the previous method.

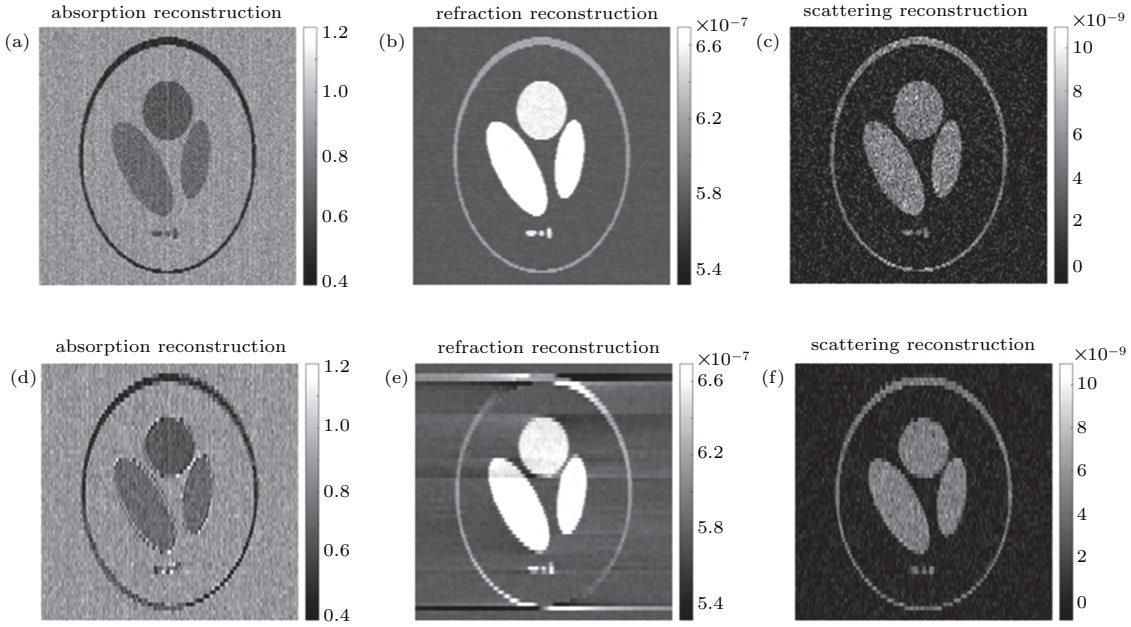


Fig. 6. Reconstructed images of the middle coronal slice of the simulated phantom shown in Fig. 3. The reconstructed absorption coefficient (a), refraction coefficient (b), and scattering coefficient (c) using the proposed imaging system, and (d)–(f) the counterparts using the previous imaging system.

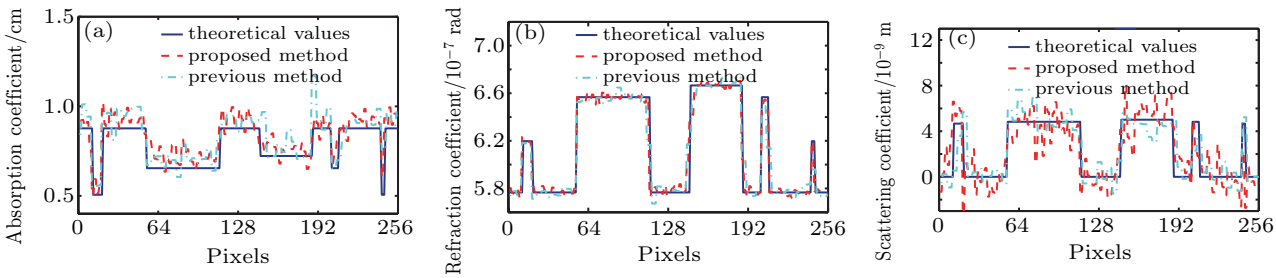


Fig. 7. (color online) Profile comparisons of the line shown in Fig. 3(b): The comparisons between the reconstructed absorption coefficient (a), refraction coefficient (b), and scattering coefficient (c), and the corresponding theoretical coefficients in the line shown in Fig. 3(b).

5. Conclusion

In this manuscript, a single-shot phase contrast imaging with better vertical spatial resolution has been proposed employing a modified staggered analyzer grating. This phase contrast imaging system can achieve phase contrast radiography without stepping the gratings, thus mechanical noise and the prolonged imaging time can be minimized. Furthermore, fast and simple x-ray phase tomography can be performed using the proposed method, which is important in the

limited radiation imaging. This work was implemented in Talbot interferometer, but it can be easily extended to other x-ray phase contrast imaging, such as Talbot–Lau interferometer and the grating-based non-interferometric phase contrast imaging. Due to the short exposure time, high stability and decent vertical spatial resolution, it may become a popular method in x-ray grating-based phase contrast imaging.

Appendix A: Derivation of the information extraction formula using the proposed imaging system

From the ASR method presented by Li *et al.* in 2016, we can know when the sample rotation angle equals to φ, the absorption, refraction and scattering information of sample can be extracted respectively as:

$$M_\varphi(x_r,y)=\ln\left[\frac{I_{\rm U}^{\rm b}(x_r,\varphi,y)+I_{\rm D}^{\rm b}(x_r,\varphi,y)}{I_{\rm U}^{\rm s}(x_r,\varphi,y)+I_{\rm D}^{\rm s}(x_r,\varphi,y)}\right], \tag{A1}$$

$$\theta_\varphi(x_r,y)=-\frac{p}{2\pi D}\left[\arctan\left(\frac{I_{\rm U}^{\rm s}(x_r,\varphi,y)-I_{\rm D}^{\rm s}(x_r,\varphi,y)}{I_{\rm V}^{\rm s}(x_r,\varphi,y)-I_{\rm P}^{\rm s}(x_r,\varphi,y)}\right)-\arctan\left(\frac{I_{\rm U}^{\rm b}(x_r,\varphi,y)-I_{\rm D}^{\rm b}(x_r,\varphi,y)}{I_{\rm V}^{\rm b}(x_r,\varphi,y)-I_{\rm P}^{\rm b}(x_r,\varphi,y)}\right)\right], \tag{A2}$$

$$\begin{aligned}\sigma_\varphi^2(x_r,y)=&-\frac{p^2}{2\pi^2D^2}\ln\left[\frac{\sqrt{(I_{\rm U}^{\rm s}(x_r,\varphi,y)-I_{\rm D}^{\rm s}(x_r,\varphi,y))^2+(I_{\rm V}^{\rm s}(x_r,\varphi,y)-I_{\rm P}^{\rm s}(x_r,\varphi,y))^2}}{V_0(I_{\rm U}^{\rm s}(x_r,\varphi,y)+I_{\rm D}^{\rm s}(x_r,\varphi,y))}\right]\\&+\frac{p^2}{2\pi^2D^2}\ln\left[\frac{\sqrt{(I_{\rm U}^{\rm b}(x_r,\varphi,y)-I_{\rm D}^{\rm b}(x_r,\varphi,y))^2+(I_{\rm V}^{\rm b}(x_r,\varphi,y)-I_{\rm P}^{\rm b}(x_r,\varphi,y))^2}}{V_0(I_{\rm U}^{\rm b}(x_r,\varphi,y)+I_{\rm D}^{\rm b}(x_r,\varphi,y))}\right],\end{aligned} \tag{A3}$$

where $I_{\rm V}^{\rm b}$, $I_{\rm U}^{\rm b}$, $I_{\rm P}^{\rm b}$, $I_{\rm D}^{\rm b}$ are projections measured at the position valley, upslope, peak and downslope respectively without sample in the system, while $I_{\rm V}^{\rm s}$, $I_{\rm U}^{\rm s}$, $I_{\rm P}^{\rm s}$, and $I_{\rm D}^{\rm s}$ are measured with sample in the system.

While using the presented imaging system, $I_{\rm D}^{\rm s}$ is acquired as the odd rows of the analyzer grating is set at the downslope position, and $I_{\rm P}^{\rm s}$ can be acquired at the same time from the even rows of the analyzer grating. Meanwhile the $I_{\rm U}^{\rm s}$ can be obtained from the odd rows as the imaging system rotated 180°. Considering two rows are defined as an extraction unit, we can obtain

$$\begin{aligned}&I_{\rm D}^{i}(x_r,\varphi,2y-1)=I_{\rm D}^{i}(x_r,\varphi,2y)=I_{\varphi}^{i}(x_r,2y-1),\\&I_{\rm P}^{i}(x_r,\varphi,2y-1)=I_{\rm P}^{i}(x_r,\varphi,2y)=I_{\varphi}^{i}(x_r,2y),\\&I_{\rm U}^{i}(x_r,\varphi,2y-1)=I_{\rm U}^{i}(x_r,\varphi,2y)\\&=I_{\rm D}^{i}(-x_r,\varphi+\pi,2y-1)=I_{\varphi+\pi}^{i}(-x_r,2y-1),\\&I_{\rm V}^{i}(x_r,\varphi,2y-1)=I_{\rm V}^{i}(x_r,\varphi,2y)\\&=I_{\rm D}^{i}(x_r,\varphi,2y-1)+I_{\rm U}^{i}(x_r,\varphi,2y-1)-I_{\rm P}^{i}(x_r,\varphi,2y-1)\\&=I_{\varphi}^{i}(x_r,2y-1)+I_{\varphi+\pi}^{i}(-x_r,2y-1)-I_{\varphi}^{i}(x_r,2y),\end{aligned}$$

where $i=$ b or s means the x ray intensities recorded without or with the sample in the imaging system.

Thus equations (A1)–(A3) can be rewritten as:

$$M_\varphi(x_r,2y-1)=M_\varphi(x_r,2y)=\ln\left[\frac{I_{\varphi}^{\rm b}(x_r,2y-1)+I_{\varphi+\pi}^{\rm b}(-x_r,2y-1)}{I_{\varphi}^{\rm s}(x_r,2y-1)+I_{\varphi+\pi}^{\rm s}(-x_r,2y-1)}\right], \tag{A4}$$

$$\begin{aligned}\theta_\varphi(x_r,2y-1)=\theta_\varphi(x_r,2y)=&-\frac{p}{2\pi D}\left[\arctan\frac{I_{\varphi+\pi}^{\rm s}(-x_r,2y-1)-I_{\varphi}^{\rm s}(x_r,2y-1)}{I_{\varphi}^{\rm s}(x_r,2y-1)+I_{\varphi+\pi}^{\rm s}(-x_r,2y-1)-2I_{\varphi}^{\rm s}(x_r,2y)}\right]\\&+\frac{p}{2\pi D}\left[\arctan\frac{I_{\varphi+\pi}^{\rm b}(-x_r,2y-1)-I_{\varphi}^{\rm b}(x_r,2y-1)}{I_{\varphi}^{\rm b}(x_r,2y-1)+I_{\varphi+\pi}^{\rm b}(-x_r,2y-1)-2I_{\varphi}^{\rm b}(x_r,2y)}\right],\end{aligned} \tag{A5}$$

$$\begin{aligned}\sigma_\varphi^2(x_r,2y-1)=&\sigma_\varphi^2(x_r,2y)\\=&-\frac{p^2}{2\pi^2D^2}\ln\left[\frac{\sqrt{(I_{\varphi+\pi}^{\rm s}(-x_r,2y-1)-I_{\varphi}^{\rm s}(x_r,2y-1))^2+(I_{\varphi}^{\rm s}(x_r,2y-1)+I_{\varphi+\pi}^{\rm s}(-x_r,2y-1)-2I_{\varphi}^{\rm s}(x_r,2y))^2}}{V_0(I_{\varphi}^{\rm s}(x_r,2y-1)+I_{\varphi+\pi}^{\rm s}(-x_r,2y-1))}\right]\\&+\frac{p^2}{2\pi^2D^2}\ln\left[\frac{\sqrt{(I_{\varphi+\pi}^{\rm b}(-x_r,2y-1)-I_{\varphi}^{\rm b}(x_r,2y-1))^2+(I_{\varphi}^{\rm b}(x_r,2y-1)+I_{\varphi+\pi}^{\rm b}(-x_r,2y-1)-2I_{\varphi}^{\rm b}(x_r,2y))^2}}{V_0(I_{\varphi}^{\rm b}(x_r,2y-1)+I_{\varphi+\pi}^{\rm b}(-x_r,2y-1))}\right].\end{aligned} \tag{A6}$$

References

[1] Pfeiffer F, Herzen J, Willner M, Chabior M, Auweter S, Reiser M and Bamberg F 2013 *Z. Für Med. Phys.* **23** 176

[2] Momose A, Yashiro W, Kido K, Kiyohara J, Makifuchi C, Ito T, Nagatsuka S, Honda C, Noda D, Hattori T, Endo T, Nagashima M and Tanaka J 2014 *Philos. Trans. R. Soc. Math. Phys. Eng. Sci.* **372** 20130023

[3] Pfeiffer F, Kottler C, Bunk O and David C 2007 *Phys. Rev. Lett.* **98** 108105

[4] Chen G H, Bevins N, Zambelli J and Qi Z 2010 *Opt. Express* **18** 12960

[5] Huang Z F, Kang K J, Zhang L, Chen Z Q, Ding F, Wang Z T and Fang Q G 2009 *Phys. Rev. A* **79** 013815

[6] Momose A, Kawamoto S, Koyama I and Suzuki Y 2004 *AIP Conf. Proc.* **716** pp. 156–159

[7] Kagias M, Wang Z, Villanueva-Perez P, Jefimovs K and Stampanoni M 2016 *Phys. Rev. Lett.* **116** 093902

[8] Zanette I, Bech M, Pfeiffer F and Weitkamp T 2011 *Appl. Phys. Lett.* **98** 094101

[9] Bevins N, Zambelli J, Li K, Qi Z and Chen G H 2011 *Med. Phys.* **39** 424

[10] Huang Z F, Chen Z Q, Zhang L, Kang K J, Ding F, Wang Z T and Ma H Z 2010 *Opt. Express* **18** 10222

[11] Wu Z, Gao K, Chen J, Wang D, Wang S, Chen H, Bao Y, Shao Q, Wang Z, Zhang K, Zhu P and Wu Z 2015 *Med. Phys.* **42** 741

[12] Wu Z, Gao K, Wang Z, Ge X, Chen J, Wang D and Pan Z 2013 *Med. Phys.* **40** 031911

[13] Momose A P 2003 *Opt. Express* **11** 2303

[14] Weitkamp T, Diaz A and David C 2005 *Opt. Express* **13** 6296

[15] Miao H, Chen L, Bennett E E, Adamo N M, Gomella A A, Deluca A M, Patel A, Morgan N Y and Wen H 2013 *Proc. Natl. Acad. Sci.* **110** 19268

[16] Zhu P, Zhang K, Wang Z, Liu Y, Liu X, Wu Z, A. McDonald S, Marone F and Stampanoni M 2010 *Proc. Natl. Acad. Sci.* **107** 13576

[17] Nesterets Y I and Wilkins S W 2008 *Opt. Express* **16** 5849

[18] Ge Y, Li K, Garrett J and Chen G H 2014 *Opt. Express* **22** 14246

[19] Wang Z, Gao K, Wang D, Wu Z, Chen H, Wang S and Wu Z 2014 *Opt. Lett.* **39** 877

[20] Li P, Zhang K, Bao Y, Ren Y, Ju Z, Wang Y, He Q, Zhu Z, Huang W, Yuan Q and Zhu P 2016 *Opt. Express* **24** 5829

[21] Wang Z T, Kang K J, Huang Z F and Chen Z Q 2009 *Appl. Phys. Lett.* **95** 094105

[22] Bao Y, Shao Q, Hu R, Wang S, Gao K, Wang Y, Tian Y and Zhu P 2016 *Radiat. Phys. Chem.* **137** 260

[23] Pfeiffer F, Bech M, Bunk O, Donath T, Henrich B, Kraft P and David C 2009 *J. Appl. Phys.* **105** 102006